Thermal properties of perovskite type oxides La0.6Sr0.4Co1-xFex03-δ (0 x 1.0)

TOHOKU UNIVERSITY

Thermal properties of perovskite type oxides $La_{0.6}Sr_{0.4}Co_{1-x}Fe_xO_{3-\delta}$ ($0 \leq x \leq 1.0$)

ペロブスカイト型酸化物$La_{0.6}Sr_{0.4}Co_{1-x}Fe_xO_{3-\delta}$($0 \leq x \leq 1.0$)の熱的性質

A dissertation submitted in partial satisfaction of the
requirements for the degree Doctor of Philosophy

in

Graduate School of Environmental Study

by

Yu-Cheol Shin

Committee in charge:

Professor Tatsuya Kawada, Chair
Professor Hiroyuki Fukuyama
Professor Koji Amezawa
Professor Keiji Yashiro

2017

DEDICATION

To my family

TABLE OF CONTENTS

List of Figures

List of Tables

Chapter 1. Introduction

1.1 Backgrounds

Throughout the world demand for energy continues to increase. Unfortunately, this demand has fairly increased use of fossil fuels which have significantly contributed to global warming. With the worldwide concerns for environment and energy security, advanced technologies for electric power generation, even in transportation, should be developed to eliminate emission and improve efficiency, thereby reducing the growing need to import fossil fuels.[1-3] One technology with high potential to satisfy these problems is the fuel cell. These systems offer potentially unpassed efficiency and essentially pollution-free operation using a fuel such as hydrogen.[4] Fuel cells are generally regarded as an indispensable means toward a hydrogen economy. Chemical energy is directly converted into electricity and heat without involving combustion cycles.[5]

The fuel cells are sorted by their electrolyte. Some fuel cells such as the proton exchange membrane fuel cell (PEMFC) and phosphoric acid fuel cell (PAFC) have an acid electrolyte while others such as the alkaline fuel cell (AFC) and the molten carbonate fuel cell (MCFC) have an alkaline electrolyte. There are also fuel cells with solid state oxide electrolytes such as solid oxide fuel cell (SOFC). Figure 1. 1.[6] shows summary of various type of fuel cells. Each of these technologies exhibits wide variations of its power density, fuel to electricity efficiency, and operating temperature.[7-10]

The solid oxide fuel cell (SOFC) is regarded as an attractive energy conversion system due to their high efficiency, modularity, fuel adaptability and low level emission.[11] The SOFC operate at high temperature (773K~1273K), therefore, natural gas fuel can be reformed within the cell stack eliminating the need for an expensive

external reforming system. Also, SOFC is highly efficient up to 70% energy efficiency when combined with gas turbine.[12] However, the high operating temperature of SOFC lead to seriously problems such as high-cost, degradation of efficiency, chemical reaction, thermal stress during operating and pure long-term stability and so on. [13-15] Such problems have limited the commercial development of SOFC. Recently, many research group have put considerable efforts toward solving these problems such as reducing operating temperature and developing new materials of components for good performance.

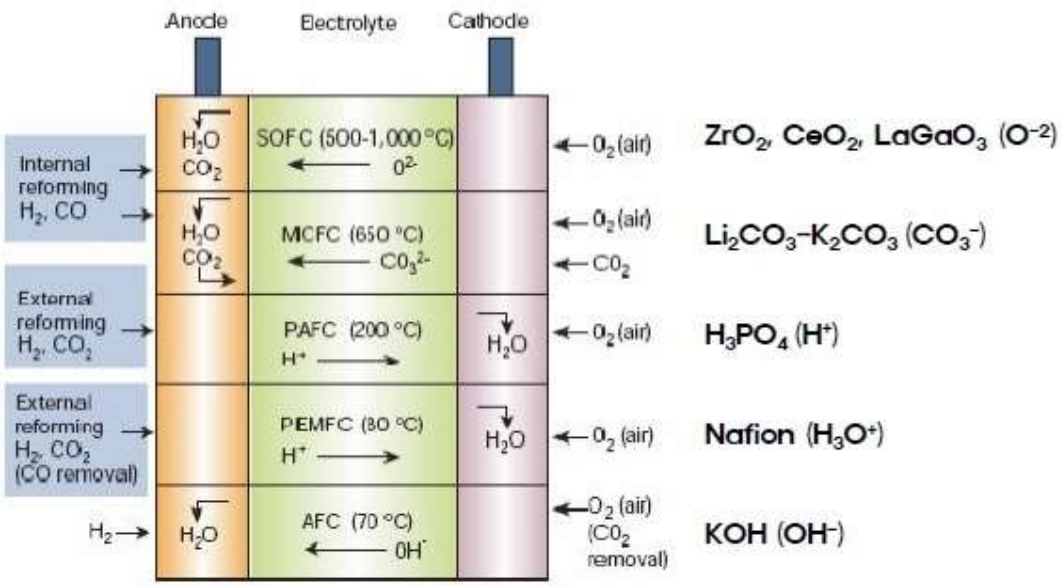

Figure 1.1. Summary of various type of fuel cells.[6]

1.2 Principle of Solid Oxides Fuel Cell (SOFC)

The simple operating principle of the SOFC is shown in Figure 1.1. SOFC is mainly composed of the anode and the cathode separated by a dense ion conducting electrolyte. Reduction of oxygen into oxygen ions occurs at the cathode (Eq.1). These ions that migrate through the electrolyte reacts with hydrogen to form water and electrons (Eq.2). These electrons then flow through an external circuit where they can do work.

Chemical reactions between SOFCs could be written in Kröger-Vink Notation as below:

Cathode: $\frac{1}{2}O_2 + 2e^{/} + V_O^{\cdot\cdot} \rightarrow O_O^x$ (1)

Anode: $H_2 + O_O^x \rightarrow H_2O + 2e^{/} + V_O^{\cdot\cdot}$ (2)

Overall: $\frac{1}{2}O_2 + H_2 \rightarrow H_2O$ (3)

where $e^{/}$electronic defect, $V_O^{\cdot\cdot}$ is a 2+ charged oxygen vacancy and O_O^x is oxygen ion on lattice.[16-17]

As mentioned earlier in Chapter 1.1, SOFC is well known as a system that offer a low pollution technology to generate electricity electrochemically with high efficiency. However, SOFC have some problems such as long-term performance stability and material selection is limited by low durability. Such problems have limited the commercial development of SOFC.[18-19] Now SOFC is still in its infancy for its commercialization. Therefore, over the past decade, many studies have been made on solve these problems of SOFC that such as mechanical properties and electrochemical properties of the SOFC components.

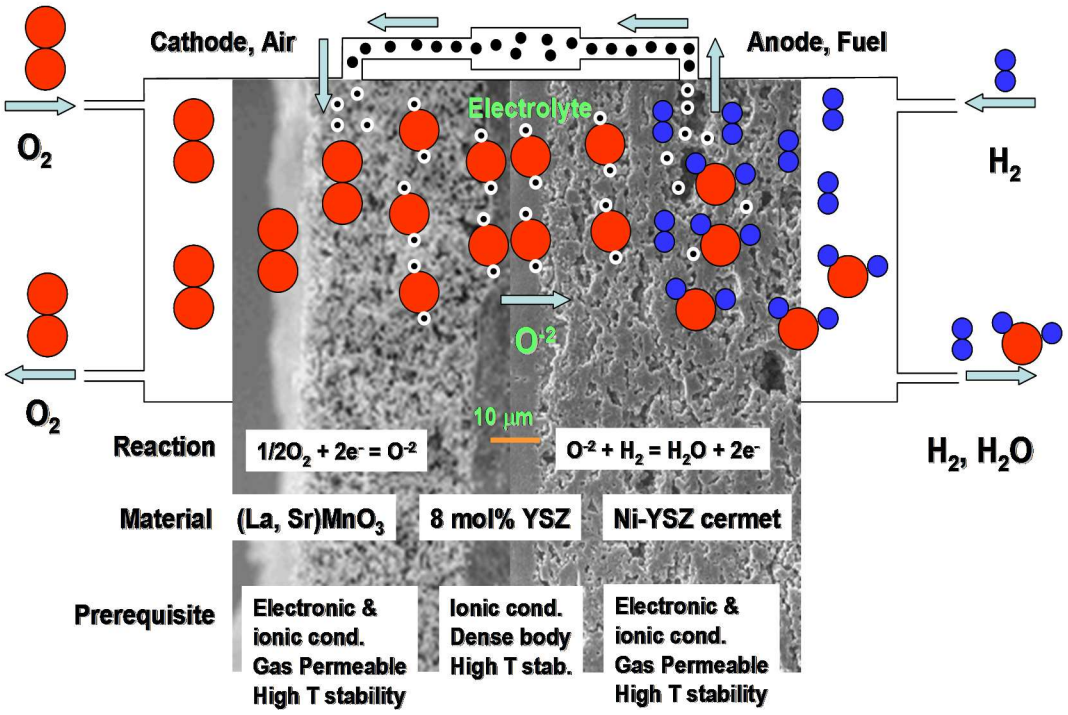

Figure 1.2. Scheme of SOFCs single cell

1.3 Perovskite-type oxide materials for cathode

Perovskite oxides is one of the most significant materials playing an important role not only in SOFCs but also gas sensor, catalysts and solar cells.[20–22] Perovskite oxides, originated from $CaTiO_3$, having the general structure ABO_3. In structure, A-site cation and B-site cation with oxygen anions, as seen as in Figure 1.3. Perovskite oxides has high structural stability, and each site cation can be substituted by a foreign cation having different oxidation state or radius. Thus, the oxidation state of A and/or B-site cation and the content of oxygen vacancy can be controlled when desired foreign cation is used, and it is able to exhibit various physical and chemical properties behaviour by dopant materials. [23–24]

Cathode materials for SOFC should satisfy the thermodynamic stability at operating temperature, high electronic conductivity, compatibility with the electrolyte and satisfactory mechanical strength.

Perovskite oxides Lanthanum Strontium Manganite (LSM) is the typical cathode materials because of its compatibility with Yttria Stabilized Zirconia (YSZ) electrolyte. LSM has high electronic conductivity, mechanical property, thermal and chemical stabilities at high operating temperature. However, the oxygen ionic conductivity of LSM is very low, which seriously restrict the use of cathode in the development of intermediate temperature SOFC (IT-SOFC).[25-26]

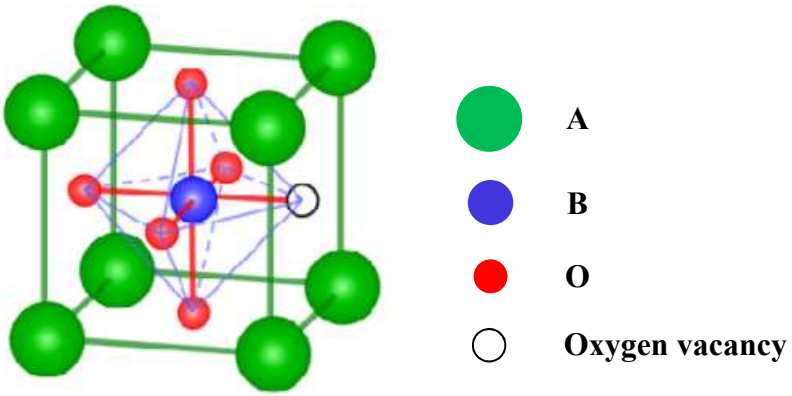

Figure 1.3. Perovskite oxide structure ABO_3.[23]

Doped rare earth elements with perovskite oxides are interesting materials for many electronic applications because of their mixed conductivity.[27-28] A and/or B site–doped rare earth elements compounds have been studied as candidates to replace the manganite and cobaltite cathodes because of its high catalytic activity and mixed ionic-electronic conductivities at intermediate temperature.[25,29] Table 1.1 shows various properties of SOFC cathodes as doped rare earth materials.

Table 1.1 Summarizes the most widely study cathode materials for SOFC

Material	TEC (K^{-1})	Resistivity		Conductivity		Diffusion		
		ASR (Ωcm^2)	T (K)	σ (S/cm)	T (K)	K^* (cm/s)	D^* (cm^2/s)	T (K)
$La_{1-x}Sr_xMnO_3$ 30-31	11.6×10^{-6}	0.18	1023	180	1073	-	3×10^{-9}	1073
$La_{1-x}Sr_xFe_{0.8}Ni_{0.2}O_3$ 32-33	15.6×10^{-6}	0.16	973	435	1073	-	-	-
$La_{0.6}Ca_{0.4}Fe_{0.8}Ni_{0.2}O_3$ 34	11×10^{-6}	0.10	1073	260	873	-	-	-
$La_{0.6}Sr_{0.4}Fe_{0.8}Cu_{0.2}O_3$ 35	14.6×10^{-6}	0.138	1023	135	548	-	-	-
$Pr_{0.6}Sr_{0.4}$ $Co_{0.2}Fe_{0.8}O_3$ 36	19.6×10^{-6}	0.046	1073	1040	573	-	9.4×10^{-5}	873
$LaNi_{0.6}Fe_{0.4}O_3$ 37-38	11.4×10^{-6}	0.018	1073	600	873	-	2×10^{-7}	1223
$Pr_{1-x}Sr_x$ $Co_{0.2}Fe_{0.8}O_3$ 39-40	14×10^{-6}	0.454	873	2190	873	-	-	-
$Sm_{0.5}Sr_{0.5}CoO_3$ 41-42	22.8×10^{-6}	0.20	873	1000	1123	6×10^{-5}	8.6×10^{-7}	1163
$PrBaCo_2O_5$ 43-45	20×10^{-6}	0.11	873	2000	423	1×10^{-3}	1×10^{-5}	623
$GdBaCo_2O_5$ 46-47	20.1×10^{-6}	0.15	1023	512	773	2×10^{-6}	3×10^{-7}	623

1.4 Perovskite-type oxides $La_{0.6}Sr_{0.4}Co_{1-x}Fe_xO_{3-\delta}$ (LSCF)

Perovskite-type oxides $La_{0.6}Sr_{0.4}Co_{1-x}Fe_xO_{3-\delta}$ (LSCF) have been extensively studied for oxygen sensors, solid oxide fuel cells and catalysts.[48-49] Perovskite-type oxides La0.6Sr0.4Co1-xFexO3-δ (LSCF) is one of most promising candidate materials for cathode of SOFC because of its high mixed ionic-electronic conductivity and fast oxygen surface reaction rate.[50] As is known, LSCF changes its crystal structure and shows oxygen nonstoichiometry and electric conductivity depending on temperature and oxygen partial pressure (PO_2). Electrical conductivity of LSCF increases to a maximum then rapidly decreases with increasing temperature. The increase in electrical conductivity at lower temperatures can be due to the increasing mobility of the localized hole via Co^{4+} and Co^{3+}, whereas decreases at higher temperatures is related to the reduction of Co^{4+} which is accompanied by formation of oxygen vacancy.

Dependence of electrical conductivity on PO_2 is described by the equilibrium reaction Eq. (4).

$$\mathbf{O_O^x} + \mathbf{2h^{\cdot}} \leftrightarrow \boldsymbol{V_O^{\cdot\cdot}} + \frac{\mathbf{1}}{\mathbf{2}}\,\mathbf{O_2} \qquad (4)$$

With increasing PO_2, the concentration of oxygen vacancies decreases and with decreasing PO_2, the concentration of vacancies increases thereby decreasing the number of electronic charge carriers and so the conductivity decrease. [51-52] It is well known that the characteristics of LSCF materials vary extensively depending on Co content. A LSCF with lower Co content has localized electrons and a higher Co content LSCF delocalized electrons. Moreover, localized and delocalized LSCF materials have quite different electrochemical properties such as oxygen vacancy concentration, thermal expansion, electrical conductivity, etc. The localized LSCF has lower electrical conductivity than delocalized LSCF. The oxygen vacancy concentration of localized LSCF is smaller than delocalized LSCF. Figure 1. 4 shows

oxygen nonstoichiometry and electrical conductivity of various LSCF compositions ($0 \leq x \leq 1.0$) as function of PO_2 and temperature. [53-54]

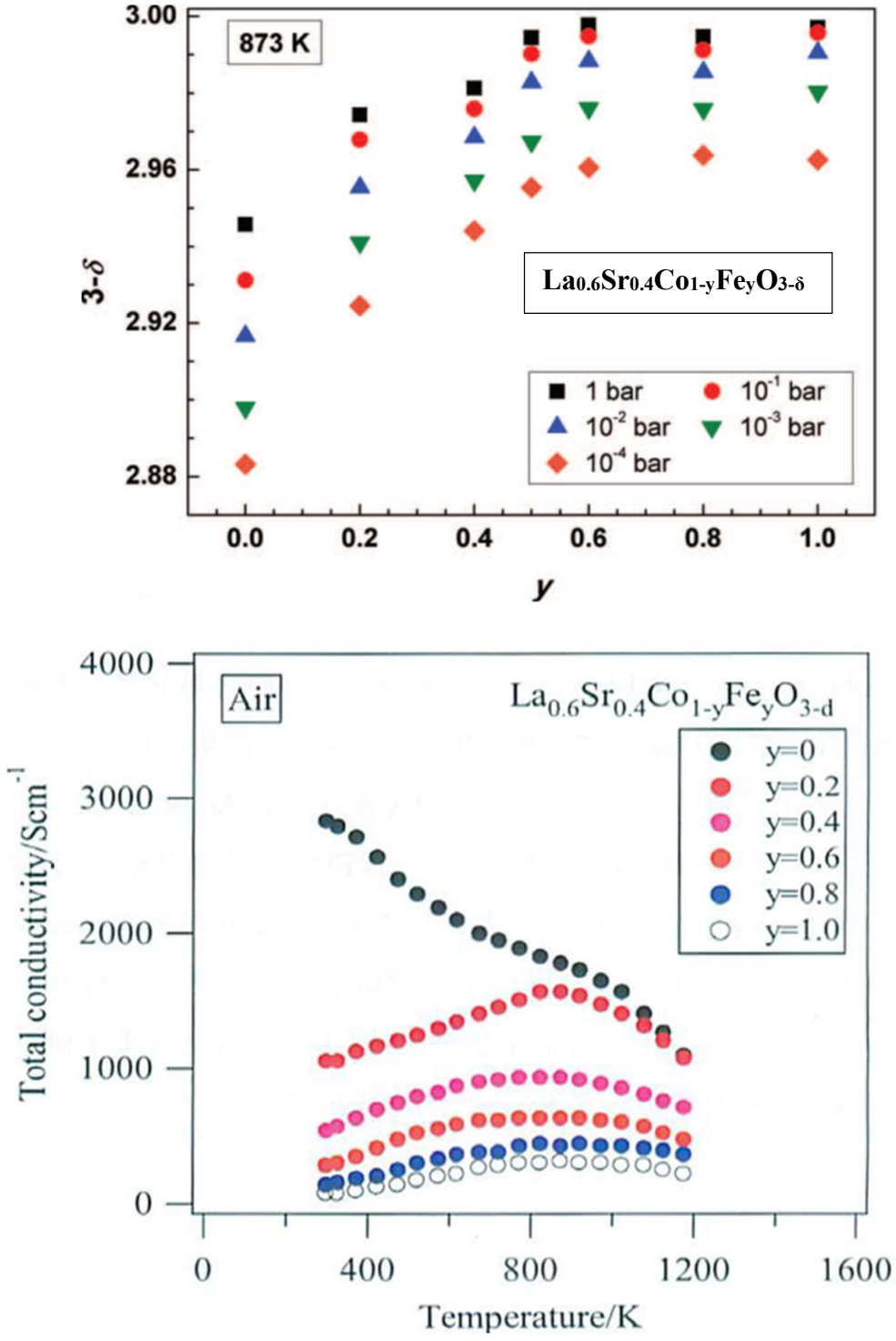

Figure 1.4. Oxygen nonstoichiometry (a) and electrical conductivity (b) of LSCF ($0 \leq x \leq 1.0$) as a function of PO_2 and temperature.[53-54]

In order to develop a commercial LSCF cathode for SOFC with high performance and long-term stability, it is important to understand temperature distribution on cell. [12,55-56] For this purpose, thermal properties of LSCF should be evaluated particularly under SOFC operating conditions, *e.g.* at elevated temperatures and under various PO_2. Although there exist several reports on the thermal properties of the LSCF, most of data are limited to thermal diffusivity, heat capacity and thermal conductivity at lower temperature range. Most of the high temperature data is focused on the such as thermal expansion or thermoelectric property.[57-59] There are limited number of reports on the thermal properties of the related materials at higher temperature range, but are only been determined in air and with different dopants in A and/or B site ($LaCoO_3$, $LaFeO_3$, $La_{1-x}Ca_xCrO_3$, $LaCo_{1-x}Ni_xO_3$). Figure 1.5 and 1.6 shows various thermal properties such as thermal diffusivity, heat capacity and thermal conductivity of localized (Figure 1.5) and delocalized system (Figure 1.6) materials.[60-62]

Thus, we aimed to investigate thermal properties of various LSCF compositions ($0 \leq x \leq 1.0$) as functions of Co content, temperature and PO_2.

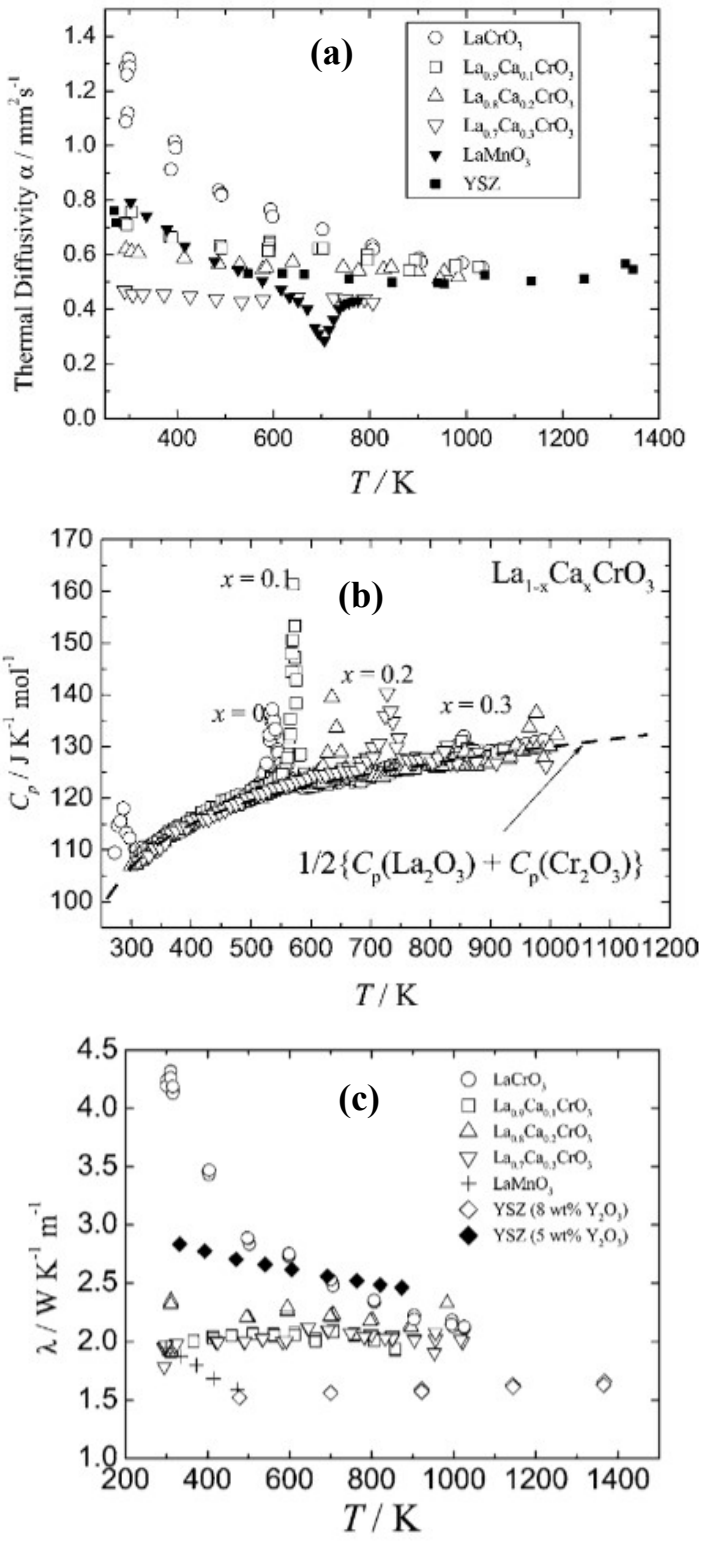

Figure 1.5. Thermal diffusivity (a), heat capacity (b) and thermal conductivity (c) of localized system materials $La_{1-x}Ca_xCrO_3$ as a function of temperature. [61]

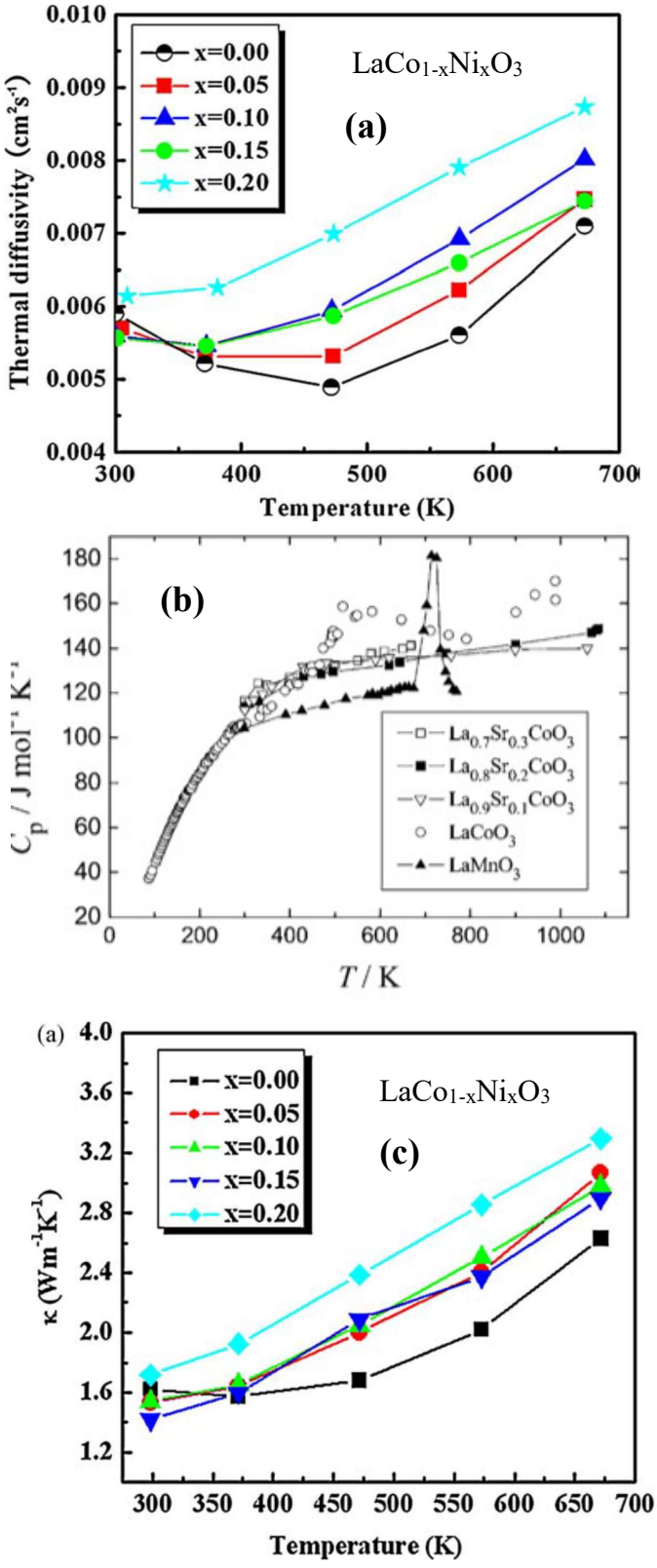

Figure 1.6. Thermal diffusivity of $LaCo_{1-x}Ni_xO_3$ (a), heat capacity of $La_{1-x}Sr_xCoO_3$ (b) and thermal conductivity of $LaCo_{1-x}Ni_xO_3$ (c) in delocalized system materials as a function of temperature. [61-62]

1.5 Object of this study

In this study, the thermal properties of Perovskite-type oxides $La_{0.6}Sr_{0.4}Co_{1-x}Fe_xO_{3-\delta}$ ($0 \leq x \leq 1.0$) are investigated, and the heat conduction mechanism of this materials will be discussed.

In Chapter 2, thermal diffusivities of $La_{0.6}Sr_{0.4}Co_{1-x}Fe_xO_{3-\delta}$ ($0 \leq x \leq 1.0$) will be investigated. The dependencies of the thermal diffusivities of LSCF on temperature, oxygen partial pressure (PO_2) and the material compositions will be discussed in terms of oxygen nonsotichiometry.

In Chapter 3, weight change and heat capacities of $La_{0.6}Sr_{0.4}Co_{1-x}Fe_xO_{3-\delta}$ (x=0, 0.8, 1.0) will be investigated by simultaneous thermogravimetry and differential scanning calorimetry (TG-DSC). The apparent dependencies of the heat capacity of LSCF on temperature will be discussed with reference to oxygen nonsotichiometry change with temperature. Moreover, heat capacities will be compared with Neumann-Kopp rule.

In Chapter 4, thermal conductivities of $La_{0.6}Sr_{0.4}Co_{1-x}Fe_xO_{3-\delta}$ (x=0, 0.8, 1.0) will be calculated using thermal diffusivities and heat capacities. It will be compared with the estimated contributions from lattice vibration (phonon) and electron, demonstrating the difference between the localized and de-localized electron system.

In Chapter 5, all results and conclusions will be summarized by chapter and general conclusions for $La_{0.6}Sr_{0.4}Co_{1-x}Fe_xO_{3-\delta}$ ($0 \leq x \leq 1.0$) will be discussed.

Chapter 2. Thermal diffusivities of Perovskite oxides $La_{0.6}Sr_{0.4}Co_{1-x}Fe_xO_{3-\delta}$ ($0 \leq x \leq 1.0$)

2.1 Introduction

Solid oxide fuel cells (SOFC) are expected as a new power generation system for high efficiency. However, several improvements are needed for practical use. Pure long-term stability is one of the most important issue.[1-2] To improve this problem, need to understand temperature distribution in the cell and stack. For this purpose, thermal properties of SOFC components should be evaluated particularly under SOFC operating conditions, *e.g*. at elevated temperatures and under various oxygen partial pressures (PO_2).

Perovskite-type oxides $La_{0.6}Sr_{0.4}Co_{1-x}Fe_xO_{3-\delta}$ (LSCF) is a potential candidate as a mixed-conducting cathode for SOFCs, and as an oxygen separation membrane material.[3-4] In order to employ these compositions either as oxide electrodes or as oxygen-permeating membranes, it is of importance to examine the oxygen deficiency and its influence on other material properties. For instance, it was reported that electrochemical and mechanical properties strongly depend on the oxygen nonstoichiometry.[5-8] However, little is known about the influence of oxygen nonstoichiometry on thermal properties. [9-11]

In this study, thermal diffusivities of the LSCF were investigated by using the laser flash method (LFA) at high temperatures up to 1173K under controlled oxygen atmospheres. Dependencies of the thermal diffusivities of LSCF on temperature, PO_2 and the material composition are discussed in terms of oxygen nonsotichiometry.

2.2 Experimental

2.2.1 Preparation of $La_{0.6}Sr_{0.4}Co_{1-x}Fe_xO_{3-\delta}$ ($0 \leq x \leq 1.0$)

Commercial lanthanum oxide (La_2O_3, Rare metallic co., Ltd, Japan), strontium (II) carbonate ($SrCO_3$, Kojundo chemical laboratory co., Ltd, Japan), cobalt (II) nitrate ($Co(NO_3)_2 \cdot 6H_2O$, Kojundo chemical laboratory co., Ltd, Japan) and Iron (III) nitrate ($Fe(NO_3)_3 \cdot 9H_2O$, Kojundo chemical laboratory co., Ltd, Japan) were used as starting materials to synthesize $La_{0.6}Sr_{0.4}Co_{1-x}Fe_xO_{3-\delta}$ (LSCF) powder depending on amounts of Co by the conventional Pechini method. Stoichiometric amounts of metal oxides and metal nitrates were first dissolved in de-ionized water to obtain a mixed solution. Subsequently, citric acid, nitric acid and ethylene glycol were added in the solution. The obtained solutions were heated to 873 K for polymer resin. At the end, the polymer resin was calcined at 1173 K. The calcined powders were ground by satellite-type ball milling for 2hrs using Al_2O_3 balls with ethanol and zirconia balls. Obtained powders were hydrostatically pressed at 150MPa into compacts, and then sintered in air at 1573K-1673K for 6h to obtain dense samples. For the thermal diffusivity measurement, the sintered compacts were cut into rectangles (c.a. 10 x 10 x 1 mm). To identify the crystal phases, calcined powders and sintered compacts of LSCF were investigated using an X-ray diffraction (XRD) analyzer with CuKα (Mac Science M18X, Japan) at room temperature. The densities of the sintered LSCF compact were carried out by digital scale with density determination kit (XSE205, METTLER TOLEDO, German). The density of LSCF was measured 5-10 times and the average was used for calculation.

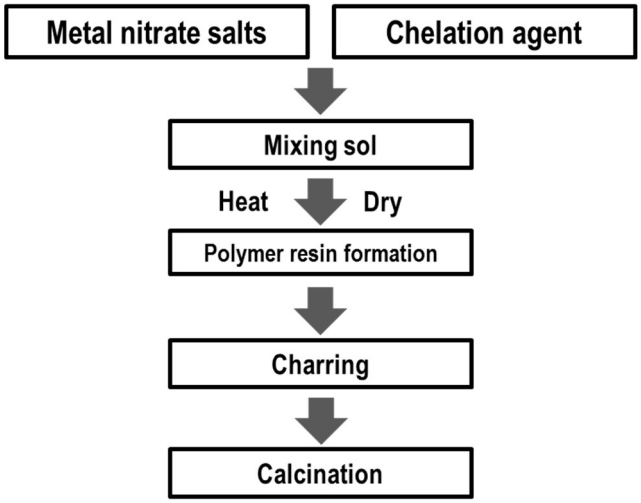

Figure 2.1. Scheme of sample preparation.

2.2.2 Thermal diffusivities of $La_{0.6}Sr_{0.4}Co_{1-x}Fe_xO_{3-\delta}$ ($0 \leq x \leq 1.0$)

The basic principle of the laser flash measurement involves rapid heating of one (bottom side in Figure 2.2) of the specimen using a single laser pulse and measuring the temperature rise on the opposite side by an IR detector, as shown in Figure 2.2. The plot of temperature rise (ΔT) at the top surface versus time is recorded for calculating thermal diffusivity at various temperatures. Then the time required for the heat to travel through the sample and cause the temperature to rise on the top surface is used to calculate the diffusivity. The thermal diffusivity can be calculated by the "t (1⁄2) method".[12] As following Parker's the measurement equation for top surface temperature as a function of time is

$$T(L,t) = 2T_f \sum_{n=1}^{\infty} \frac{\gamma_n^2(\gamma_n^2+l^2)\cos\gamma_n}{\gamma_n^2+l^2+2l} \exp(-\gamma_n^2 D\, t/L^2) \qquad (1)$$

where, T_f is the final sample temperature, D is the thermal diffusivity, L is the sample thickness and l is the heat loss factor.

Eq. (1) can be applied when the following conditions are satisfied: the laser pulse width is negligibly short and there is no heat loss during measurement after pulse heating, i.e. l = 0. Because, the heating of the top surface can no longer be considered instantaneous relative to the time for the heat to diffuse through the sample. Therefore, Eq. (1) can be expressed as

$$\alpha = 0.13879 \frac{L^2}{t_{1/2}} \quad (2)$$

where, $t_{1/2}$, is the time required for the top surface to reach half of the maximum temperature rise.

The measurements of thermal diffusivities of LSCF ($0 \leq x \leq 1.0$) were carried out by laser flash apparatus (LFA457, NETZCH, German) as a function of oxygen partial pressure, PO_2 (0.2 bar to 10^{-4} bar) and temperature (773K to 1173K). In order to control the atmospheres, a gas mixing system and an oxygen sensor are additionally attached to the LFA. Measurements were repeated until the obtained thermal diffusivity reach to the constant value at each temperature and PO_2.

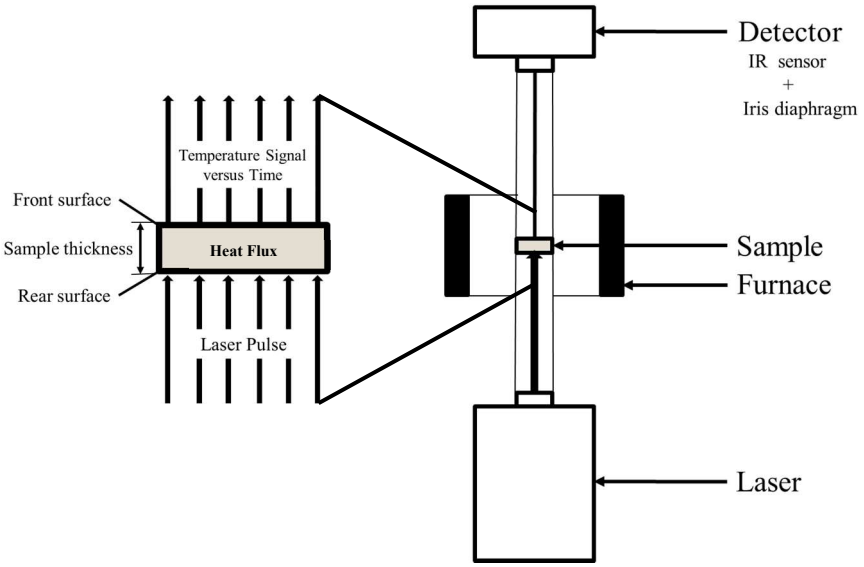

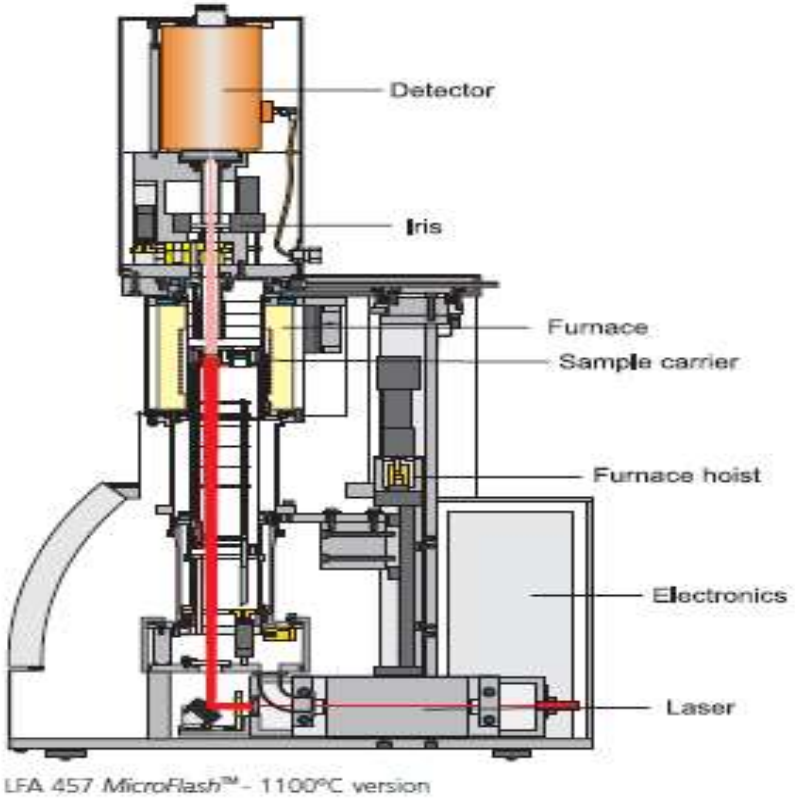

Figure 2.2. Scheme of LFA device.

Chapter 3. Weight loss (TG) and heat capacity (*C*p) of perovskite oxides $La_{0.6}Sr_{0.4}Co_{1-x}Fe_xO_{3-\delta}$ (x = 0, 0.8, 1)

3.1 Introduction

In Chapter 2, it was found out that the thermal diffusivities of LSCF are significantly affected by the oxygen nonstoichiometry. The thermal diffusivity of LSCF decreased with the decrease in oxygen deficiency (δ) at all investigated temperatures and PO_2. It means that the thermal diffusivity of LSCF showes a one-to-one relation with the oxygen deficiency concentration (δ). Further discussion is to be made on thermal conductivity. This chapter focuses on the measurement of heat capacity (Cp) because they are indispensable to calculate for thermal conductivity.

Several studies have already been conducted to measure the heat capacity of $La_{1-x}Sr_xCo_{1-y}Fe_yO_{3-\delta}$, especially at lower temperature range.[1-2] At higher temperature range, however, the heat capacity has only been determined for an air atmosphere and a few or non-dopant in A and/or B site ((x, y=0; $LaCoO_3$), (x=0, y=1; $LaFeO_3$), (x=0.1, y=0; x=0.2, y=0; x=0.3, y=0)). The heat capacity of LSCF have been reported to a rather limited extent.[3-5]

In this chapter, therefore, we will discuss with heat capacity of $La_{0.6}Sr_{0.4}Co_{1-x}Fe_xO_{3-\delta}$ (x =1.0, 0.8, 0) as function of temperature and PO_2. The TG and heat capacities of the LSCF were investigated by using the TG-DSC at high temperatures up to 1273K under controlled oxygen atmospheres.

3.2 Experimental

3.2.1 Preparation of $La_{0.6}Sr_{0.4}Co_{1-x}Fe_xO_{3-\delta}$ (x =0, 0.8, 1)

Perovskite oxides $La_{0.6}Sr_{0.4}Co_{1-x}Fe_xO_{3-\delta}$ (x =1.0, 0.8, 0) were synthesized by the Pechini method. Stoichiometric amounts of La_2O_3, $SrCO_3$, $Co(NO_3)_2 \cdot 6H_2O$ and $Fe(NO_3)_3 \cdot 9H_2O$ were completely dissolved in nitric acid solution. Subsequently, citric acid and ethylene glycol were added to the solution. The obtained solutions were heated on a hot plate under regular stirring to 873K for polymer resin. At the end, the polymer resin was calcined at 1173K. Obtained powders were hydrostatically pressed at 150 MPa into compacts, and then sintered in air at 1573K-1673K for 6 h to obtain dense samples. For the TG-DSC measurement, the sintered compacts were cut into a smaller piece than Pt crucible. The relative densities of the sintered LSCF compacts were always higher than 95%. The density of sintered samples was obtained by using Archimedes measurement. The phase of sintered samples was characterized by XRD to confirm no phase change after sintering.

3.2.2 TG-DSC Measurement for weight loss (TG) and heat capacity (C*p*) of $La_{0.6}Sr_{0.4}Co_{1-x}Fe_xO_{3-\delta}$ (x =0, 0.8, 1)

The weight loss (TG) and heat capacity (*C*p) of LSCF were measured using thermogravimetry-differential scanning calorimetry (TG-DSC). In this study, the heat capacity of LSCF sintered samples was measured by using the STA 449 F1 TG-DSC system (NETZSCH, German) in the oxygen partial pressure range from 0.2 bar to 10^{-4} bar and in the temperature range from R.T to 1273K. The PO_2 was controlled by mixing gases with oxygen sensor. In STA 449 F1 system, heat capacity of the LSCF under investigation can be calculated by a simple comparison of the heat flow rates in three steps: (1) “baseline” step, the dissymmetry of the apparatus is evaluated by putting two empty crucibles of identical masses in the sample and reference sides of

the calorimeter. The sample in the reference side is kept in place for all the subsequent experiments. (2) “calibration” step, the crucible loaded with the standard material (in this study used sapphire) is put on the sample side. (3) “actual sample measurement” step, the crucible loaded with LSCF compact is put on the sample side. In these three measurement was must be constant heating rate. Shown in Figure 3.1 is simple schematic diagram of TG-DSC device.

The heat capacity of the sample was calculated from

$$Cp_{\cdot\text{sample}}\,(\text{T}) = \frac{m_{\text{ref}}}{m_{\text{sample}}}\left(\frac{V_{\text{sample}}(\text{T}) - V_{\text{base}}(\text{T})}{V_{\text{ref}}\,(\text{T}) - V_{\text{base}}(\text{T})}\right) Cp_{\cdot\text{ref}}\,(\text{T}) \qquad (1)$$

where, V_{base}, V_{ref} and V_{sample} represent heat flow during each step, respectively, *C*p sample (T) and *C*p ref (T) the heat capacities of sample and reference material, *m* sample and *m* ref represent the masses of sample and reference, respectively. In this study, Pt crucible was used with lid and sapphire was used as the refence material.

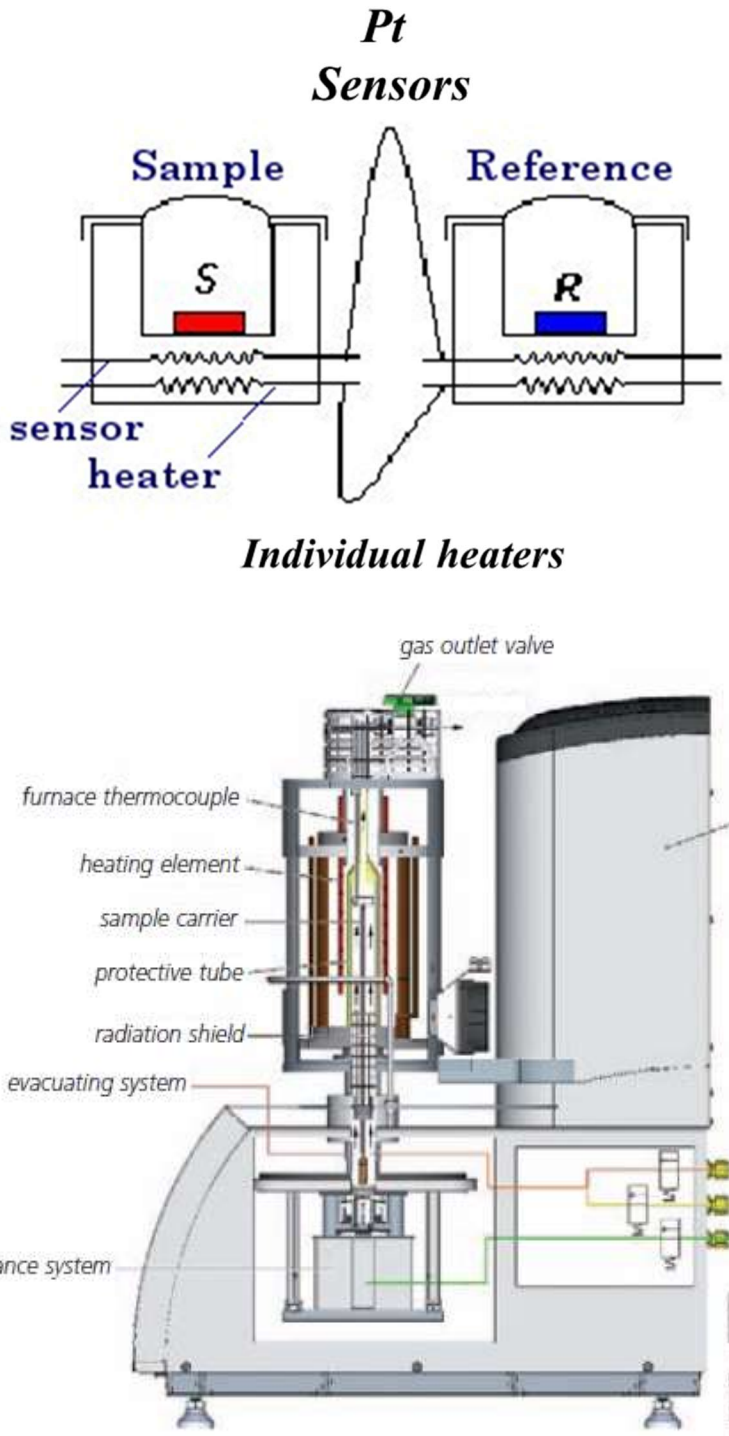

Figure 3.1. Scheme of TG-DSC

Chapter 4. Thermal conductivity and thermal conduction mechanism of $La_{0.6}Sr_{0.4}Co_{1-x}Fe_xO_{3-\delta}$ (x = 0, 0.8, 1)

4.1 Introduction

In Chapter 2 and 3, we already discussed the thermal diffusivities and heat capacities of LSCF. We found out that the thermal diffusivities of LSCF is significantly affected by the Co content and oxygen nonstoichiometry. Since heat is transported via lattice vibration and electronic charge carriers, the contributions of those two mechanisms should be clarified for better understanding. Thermal conductivity is a material property describing the ability to conduct heat.

In this chapter, the thermal conductivities of $La_{0.6}Sr_{0.4}Co_{1-x}Fe_xO_{3-\delta}$ (x =0, 0.8, 1.0) are calculated using the thermal diffusivities, heat capacities, and sintered densities. The dependence of thermal conductivity on temperature, PO_2 and Co content will be summarized. In addition, thermal conduction by phonons (lattice vibration wave) (k_p) and electrons (k_e) will be estimated from the reported values of mean free path of phonons and electronic conductivities. The calculated sum of k_p and k_e of LSCF will be compared with the measured thermal conductivities.

4.2 Experimental

4.2.1 Thermal conductivity of $La_{0.6}Sr_{0.4}Co_{1-x}Fe_xO_{3-\delta}$ (x =0, 0.8, 1.0)

The thermal conductivity (*k*) of LSCF is calculated by using Eq. (1). α: thermal diffusivity of LSCF with respect to temperature, ρ: the density of sintered LSCF sample and *C*p: heat capacity of the LSCF as a function of temperature.

$$\boldsymbol{k = \alpha \cdot p \cdot Cp} \qquad (1)$$

In this study, α, ρ and *C*p were taken from the results shown in the previous chapters. The *C*p of LSCF, which was estimated by removing the contribution of oxygen vacancy formation, was assumed to be independent of PO_2.

4.2.2 Thermal conduction mechanism in LSCF

As mentioned above, heat conduction is the transfer of heat by phonons (lattice vibrations) (*k*p) and movement of electrons (*k*e) within a body. In all materials has heat conduction by lattice vibrations (*k*p) and only in electrically conducting materials, i.e. metals, has heat conduction by electron movement (*k*e).[1-2]

In this study, calculated the thermal conductivities of phonons (lattice vibration wave) (*k*p) and electrons movement (*k*e).

The heat transfer by lattice vibration wave, *k*p, in solid can be expressed from the kinetic theory gases as:

$$k_p = \frac{1}{3} Cvl \qquad (1)$$

where, C is heat capacity (concentration x heat capacity), v is average group velocity of the wave, l is a scattering mean free path. Eq. (1) can be expressed as

$$k_p = \frac{Cpul_p}{3v_m} \qquad (2)$$

where, *C*p is heat capacity, u is sonic velocity in solid. l_p is mean free path and v_m is molar volume. This study used *C*p obtained in the previous chapter, and u is calculated from

$$u = \sqrt{\frac{E}{\rho}} \qquad (3)$$

where, ρ is density of sample and *E* is Young's modulus. The temperature dependence of Young's modulus was taken from the paper by Kimura et al.[3] Since the mean free path of phonon l_p is not known, it was assumed to be same as the reported values for $LaCrO_3$, 3Å (3 x 10^{-10} m),[4] comparable to the size of unit cell of pseudo cubic perovskite oxides.

The heat transfer by electron movement, *k*e, in solid is calculated by Wiedemann-Franz law.[5] A Wiedemann–Franz law predicts the ratio of the electronic contribution of the thermal conductivity (*k*) to the electrical conductivity (σ) of a metal is proportional to the temperature as:

$$\mathrm{L} = \frac{k_e}{\sigma T} \qquad (4)$$

where, L is constant Lorenz number (2.44 x 10^{-8} $W\Omega K^{-2}$) and σ is electrical conductivity. The electrical conductivity of LSCF was taken from the reference paper by Nakano.[6]

VITA

2007 Bachelor of Science, Chonnam National University, Gwangju, South Korea.

2009 Master of Science, Chonnam National University, Gwangju, South Korea.

2017 Doctor of Philosophy, Tohoku University, Sendai, Japan.

Publications

Y.C. Shin, S. Hashimoto, K. Yashiro, K. Amezawa, T. Kawada, "Thermal properties of perovskite-type oxides $La_{0.6}Sr_{0.4}Co_{1-x}Fe_xO_{3-\delta}$ ($0 \leq x \leq 1.0$)", ECS Transactions, 72[7], 2016, 105-110

Y.C. Shin, S. Hashimoto, K. Yashiro, K. Amezawa, T. Kawada, "Thermal diffusivities of perovskite-type oxides $La_{0.6}Sr_{0.4}Co_{1-x}Fe_xO_{3-\delta}$ ($0 \leq x \leq 1.0$)", "in preparation".

Y.C. Shin, S. Hashimoto, K. Yashiro, K. Amezawa, T. Kawada, "T Thermal conductivity of perovskite-type oxides $La_{0.6}Sr_{0.4}Co_{1-x}Fe_xO_{3-\delta}$ (x=0, 0.8, 1)", "in preparation".

Presentations and Posters

Y.C. Shin, A. Unemoto, K. Amezawa, T. Kawada, "Thermal properties of perovskite-type $La_{0.6}Sr_{0.4}Co_{1-x}Fe_xO_{3-\delta}$", The Electrochemical Society of Japan, 1E26, Kanagawa, Japan,2^{th}-3^{th}, September, 2010.

Y.C. Shin, A. Unemoto, K. Amezawa, T. Kawada, "Influence of oxygen nonstoichiometry change on thermal diffusivities of $La_{0.6}Sr_{0.4}Co_{1-x}Fe_xO_{3-\delta}$ ($0 \leq x \leq 1.0$)", The Electrochemical Society of Japan, 1C02, Niigata, Japan, 9^{th}-11^{th}, September, 2011.

Y.C. Shin, A. Unemoto, S. Hashimoto, K. Amezawa, T. Kawada, "Influence of Oxygen Nonstoichiometry Change on Thermal Properties of $La_{0.6}Sr_{0.4}Co_{1-x}Fe_xO_{3-\delta}$", Eighth International Conference on Flow Dynamics, PS4-31, Sendai, Japan, 9^{th}-11^{th}, November, 2011.

Y.C. Shin, A. Unemoto, S. Hashimoto, K. Amezawa, T. Kawada, "Thermal diffusivities of $La_{0.6}Sr_{0.4}Co_{1-x}Fe_xO_{3-\delta}$ under SOFC operation conditions", The 20th Symposium on Solid Oxide Fuel Cells in Japan, 166C, Tokyo, Japan, 12^{th} -13^{th}, December, 2011

Y.C. Shin, S. Hashimoto, K. Yashiro, K. Amezawa, T. Kawada, "Thermal properties of perovskite-type $La_{0.6}Sr_{0.4}Co_{1-x}Fe_xO_{3-\delta}$ (x=0-1.0)", The 41th Symposium on Solid State Ionis of Japan, 1C-04, Sapporo, Japan, 25th -27th, November, 2015.

Y.C. Shin, S. Hashimoto, K. Yashiro, K. Amezawa, T. Kawada, "Thermal properties of perovskite-type oxides $La_{0.6}Sr_{0.4}Co_{1-x}Fe_xO_{3-\delta}$ ($0 \leq x \leq 1.0$)", 229th ECS Meeting, IO2-1374, San Diego, USA, May 29th -June 2th, 2016.